FUEL MASS OPTIMIZATION FOR A TRISO-BASED LUNAR NUCLEAR REACTOR

An Undergraduate Research Scholars Thesis

by

LOGAN JEFFERY [1], DINYAR KADKHODAIAN [2], AND MORGAN ROGERS [3]

Submitted to the LAUNCH: Undergraduate Research office at
Texas A&M University
in partial fulfillment of the requirements for the designation as an

UNDERGRADUATE RESEARCH SCHOLAR

Approved by
Faculty Research Advisor Dr. John R. Ford

May 2021

Majors: Nuclear Engineering [1,2,3]
Physics [1]

TABLE OF CONTENTS

ABSTRACT

Fuel Mass Optimization for a TRISO-Based Lunar Nuclear Reactor

Logan Jeffery [1], Dinyar Kadkhodaian [2], and Morgan Rogers [3]
Department of Nuclear Engineering [1,2,3]
Department of Physics and Astronomy [1]
Texas A&M University

Research Faculty Advisor: Dr. John R. Ford
Department of Nuclear Engineering
Texas A&M University

This project investigates the use of low enriched uranium tristructural-isoptropic (TRISO) fuels in a potential lunar and martian nuclear reactor with the primary objective of minimizing overall reactor mass. Extraterrestrial power source options are significantly restricted by their mass, as chemical-driven launches into orbit are expensive and size-restricted. Since nuclear power sources are widely considered to be the only potential means of electricity generation for habitation in space, the mass constraint has become a particularly important issue to be addressed. These fuels were developed during the Generation-IV initiative, and are presently the subject of great interest within the nuclear community. TRISO boasts promising results in burnup, longevity, heat resistance, and safety. Therefore, this team believes that research in the use of TRISO for space applications should be further explored.

In this study, present-day core fuel assemblies and materials typically used in high temperature gas small modular reactors are analyzed and adapted to the low-gravity lunar environment while attempting to meet a 20 wt% enrichment constraint. Using a uranium oxycarbide TRISO particle, an experimental reactor system is optimized to minimize the mass of the assembly, while maintaining a critical core. The design goal of the project aims to limit the overall mass of the re-

actor at a maximum of 3500 kg, and maintain a power level of 10 kW for a minimum of 10 years. Particular design emphasis is focused on the use of low enriched uranium as a fission source, since previous highly-enriched uranium designs have come under scrutiny for proliferation concerns. This project explores the design of a low-mass, low-enriched uranium TRISO fuel reactor core that has been specialized for lunar and martian habitation and exploration. The project concludes with an analysis of the effect that uranium enrichment had on meeting the design constraints, such as mass, power output, and lifetime.

ACKNOWLEDGMENTS

Contributors

We would like to thank our faculty advisor, Dr. John R. Ford, for his support and encouragement throughout the course of this research. His guidance proved to be invaluable, and frequent meetings with him helped keep us on track and organized. We are incredibly appreciative for his contribution.

We also acknowledge the support and direction of faculty members within the Nuclear Engineering department at Texas A&M University. Dr. Karen Kirkland helped us consider vital engineering constraints. Much of this work was initially inspired by the requirements for her Engineering Analysis courses (NUEN 406/410). Dr. Sunil Chirayath's proficiency with Los Alamos National Lab's MCNP6.2 (and Vised) helped us to develop our first working pebble bed model. We are grateful for their contributions to our project.

Finally, we would like to thank our families for their encouragement and patience throughout this research. All other work conducted for this thesis was completed by students independently, while practicing social distancing during the COVID-19 pandemic.

Funding Sources

This project was unfunded.

NOMENCLATURE

AGR	Idaho National Lab's Advanced Gas Reactor
at%	Atom percent
BeO	Beryllium oxide
CO	Carbon monoxide
CO_2	Carbon dioxide
DOE	U.S. Department of Energy
Gen-III	Generation III
Gen-IV	Generation IV
E_r	Energy released per fission reaction
HALEU	High-Assay Low-Enriched Uranium
HEU	Highly enriched uranium
HTGR (VHTGR)	(Very) High temperature gas reactor
iPyC	Inner layer of pyrolytic carbon
k_{eff}	Effective multiplication factor
KRUSTY	Kilowatt Reactor Using Stirling Technology
LEU	Low-enriched uranium
MCNP	Monte Carlo N-Particle Transport Code System
N_A	Avogadro's Number (6.022e23)
oPyC	Outer layer of pyrolytic carbon
PWR	Pressurized water reactor
PyC	Pyrolytic carbon
SiC	Silicon carbide
SLS	Space Launch System

SS-304	Stainless steel 304
TiC	Titanium carbide
TiN	Titanium nitride
TRISO	Tristructural-isoptropic
UC	Uranium monocarbide
U_2C_3	Uranium sesquicarbide
UC_2	Uranium acetylide (dicarbide)
UCO	Uranium oxycarbide
UN	Uranium mononitride
U_2C_3	Uranium sesquinitride
UC_2	Uranium dinitride
U	Uranium metal
UO2	Uranium dioxide
wt%	Weight percent
Q_{th}	Volumetric heat generation
ZrC	Zirconium carbide
ZrN	Zirconium nitride
η	Efficiency (of a thermodynamic cycle)
σ_n	Microscopic cross section, where n is absorption, scattering, fission, etc.
ϕ	Neutron flux
χ_f	Neutron fission energy spectrum

1. INTRODUCTION

1.1 Motivation

Nuclear energy sources have long been accepted to be the only feasible means to power long-term extraterrestrial exploration and habitation because of their reliability, low fuel consumption rate, and long operational lifetime. Nuclear power offers a form of energy that can be operated almost entirely independently from the surrounding environment, and is not restricted by limitations in current energy storage technology.

In 2010, researchers from the U.S. National Aeronautics and Space Administration (NASA) and the U.S. Department of Energy (DOE) conducted a thorough investigation into an optimal design for small fission power systems to be used in unspecified future NASA missions [3]. The design was given specific operation parameters, including a 10-kW power output, a 15-year reactor lifetime, a mass restriction of 3500 kg, and the goal to launch within a decade [1][3]. This research helped found the Kilopower Project, which was responsible for developing the KRUSTY reactor in 2018. KRUSTY was designed to be part of NASA's current Artemis Program, with the intent of providing power to a long-term research facility on the lunar surface [5]. Its construction featured a 1-kW power output, a single B_4C control rod, and a liquid sodium coolant with a Stirling engine power conversion system [4]. It was also specifically designed to be light-weight, boasting a total mass of 1500 kg with a reactor core mass of only 134 kg. This was done by making use of a 93 wt% HEU, 7 wt% Mo fuel.

The reliance on highly-enriched uranium (HEU) fuel in this design introduces a proliferation risk, and would set a precedent for HEU usage in space. As a direct response to these concerns, the White House issued a set of standards in 2019 for all nuclear material usage in space (referred to as SPD-6) [2]. These standards included a 20% U-235 fuel enrichment limitation, meaning that progress made on KRUSTY had to be entirely discontinued. The ongoing Artemis program relies on a 2027 deadline to assemble a functioning reactor on the moon [5]. Therefore, in September

of 2020, NASA and the DOE released an industry proposal request for a low enriched uranium (LEU) core design to fuel a compact lunar power system [1].

Current concepts for conventional LEU cores make these power systems significantly more expensive to launch into space. To further complicate the issue, NASA set several strict standards on proposed designs, including a preferred 2000 kg total mass (no more than 3500 kg) and the preference to launch and land as one unit [1][11]. The nuclear power system must also be designed for compatibility with the Martian environment, provide 10 kW of electric power, and be remotely operated from Earth.

1.2 HTGRs and TRISO Fuel

The answer to NASA's strict mass limitations could lie in Generation IV (Gen-IV) reactor concepts, which are currently being studied to quickly replace the terrestrial fleet. In particular, high-temperature gas-cooled reactors (HTGRs) show promise to meet the needs of space nuclear power [9]. As the name indicates, these reactors are designed to operate at much higher temperatures than conventional reactors. HTGRs typically feature a closed Brayton cycle, where the higher operating temperatures can greatly improve efficiency. These reactors are typically helium gas-cooled, which is a lighter cooling system concept than most alternatives. They are also compatible with Stirling engines, which have historically been preferred by space research scientists as they do not require heavy turbine equipment for thermal conversion [6]. The two main HTGR core types are pebble-bed reactors and prismatic-block reactors.

Both of these variations are made up of tristructural-isotropic (TRISO) fuel particles. These fuel particles have traditionally been millimeter-scale uranium oxide/carbide kernels that are encased in several layers of pyrolytic carbon (PyC). Depending on the reactor configuration, these pellets are assembled into either fuel spheres (pebbles) or cylinders (prisms) to be used in their respective reactor cores.

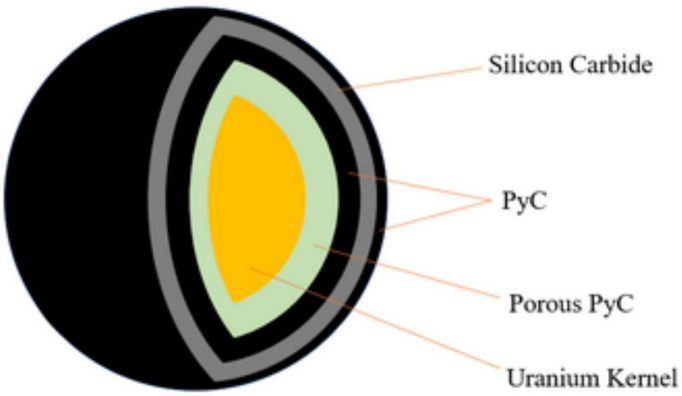

Figure 1.1: Diagram of typical TRISO layered fuel particle

Because of the use of TRISO fuels, HTGRs have an increased intrinsic safety compared to alternatives for nuclear fuel in space. In the event of a containment breach, the fuel is self-contained and able to maintain integrity at high temperatures rather than melting. The fuel structure has set records on maximum burnup, stretching the proposed lifetime to almost double that of a typical LWR (which needs to be refueled every 12-18 months) [8][20]. This is an especially remarkable feature as a moon-based reactor would have limited opportunities to refuel. TRISO-based fuel could be used in a solid-core reactor which would have an additional safety element for launch accidents. The solid core would aid in mass optimization, although criticality simulation is needed in order to compare safety-to-mass optimization.

Although the use of terrestrial TRISO fuels in HTGRs is still gaining traction, significant data exists which argues that TRISO fuel is a notable candidate for nuclear power in space. It is a fuel source that potentially meets the strict mass-to-power output requirements desired for space research and habitation. This project investigates how TRISO could contribute to the mass problem discussion by manipulating present TRISO-based fuel designs in order to optimize the mass of an extraterrestrial reactor. This research could potentially benefit other areas of space nuclear research as well.

2. TRISO PARTICLE MASS OPTIMIZATION

In this section, the design of an individual TRISO particle is investigated. Particle design manipulations are conducted to minimize the mass of an extraterrestrial HTGR by considering their effect on overall reactivity and potential modes of failure. These variations fall into one of three categories, including manipulations of the kernel fuel material, the layer materials, or the layer thicknesses. An "optimized" TRISO particle for power production in space should feature a low mass-to-power output ratio and low fuel consumption (i.e. high burnup).

For comparative purposes, these manipulations were made on a pebble-bed reactor design that will be introduced and discussed in Section 3. This section concludes with a particle design that will be used in a reactor core model, and preference is given to current designs that have experimental performance validation.

2.1 Kernel Fuel Materials

The Executive announcement from 2019 that addressed nuclear power in space (SPD-6) reduced the permissible enrichment of potential nuclear fuels to LEU [2]. LEU has been defined as a maximum of 20 wt% U-235. Before this announcement, nearly all domestic space reactor proposals were based on HEU fuel. Terrestrial HTGRs have been used to test many plutonium- and thorium-based fuels, although commercial reactors have not generally branched out of uranium kernels. However, the specification of LEU does not limit the type or amount of fuel additives, or secondary elements that can be included in the fuel composition. In fact, several fuel alternatives have been studied for use in coated particle fuel. UO_2 has also been studied with metal additives as an HTGR fuel, although these studies are not common and very few have any associated experimental data.

In general, the best fuels for space applications exhibit a high burnup at operating temperature, show the least amount of degradation over time, and have high fuel loading. The following table displays the fuel variants that were considered.

Table 2.1: List of fuel variants along with respective densities and melting points [34][36]

Material	**Symbolic**	**Density**	**Melting Point (C)**
Uranium Dioxide	UO_2	10.97	22865
Uranium Oxycarbide or "UCO"	$U(O_2,C_X)$	-	-
Uranium Carbide	UC	13.63	2550
Uranium Sesquicarbide	U_2C_3	12.88	No Data
Uranium Acetylide (Dinitride)	UC_2	12.13	2308
"UCN"	$U(C_X,N_X)$	-	-
Uranium Mononitride	UN	11.3	2577
Uranium Sesquinitride	U_2N_3	11.3*	900-1100 (Decomposes to UN)
Uranium Dinitride	UN_2	11.3*	900-1100 (Decomposes to UN)

In Table 2.1, "*" indicates that the density was treated as that of UN since the fuel decomposes to UN at HTGR operating temperatures. The following plot is a comparison of the thermal conductivity between these various fuel types as a function of temperature.

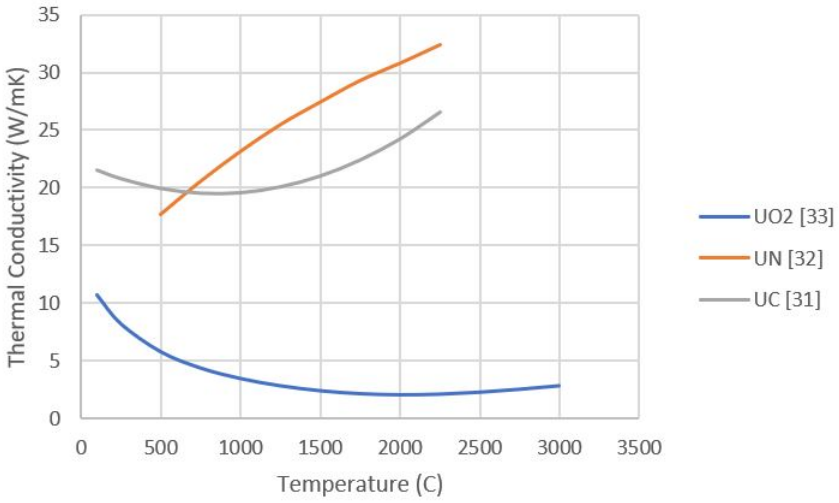

Figure 2.1: Plot comparing thermal conductivity for fuel variants

This list of fuel material candidates was run through a model of a potential TRISO-based reactor core (as introduced and described in Section 3). Table 2.2 shows how the core reactivity

was affected by the use of varying fuel types. Note that the core was designed to sustain criticality with UO_2-based fuel kernels, and that rotating reflectors were added to vary this reactivity.

Table 2.2: Fuel kernel material effect on core design reactivity

Material	**Keff**	**Reactivity**
UO_2	1.00041 ± 0.00057	0.0004098
$U(O_2,C_X)$	-	-
UC	1.04525 ± 0.00043	0.0432911
U_2C_3	1.03375 ± 0.00046	0.0326481
UC_2	1.02116 ± 0.00045	0.0207215
$U(C_X,N_X)$	-	-
UN	1.00344 ± 0.00044	0.0034282
U_2N_3	0.99555 ± 0.00044	-0.0044699
UN_3	0.98531 ± 0.0004	-0.014909

In this table, the reactivities associated with UCO and UCN are dependent on the relative abundance of the oxygen or nitrogen to the carbon. The table indicates that the change in core reactivity is fairly insignificant from fuel variant to fuel variant. This was expected, as the working fissile material is identical in each case (20 wt% enriched uranium). However, there are clear correlations associated with the secondary fuel elements and their stoichiometries. Specifically, the stoichiometry with the highest uranium-to-O/C/N ratio yielded the highest reactivity. There is also a slight tendency for the carbon-based fuels to produce a higher reactivity. Generally, the reactivity is only marginally affected by the additional secondary atoms, which follows a direct dependence on fuel loading. Since the change in fuel loading between materials is not very large, the fuel material used in a mass-optimized design is much more dependent on the unique material

characteristics.

Burnup data quantifies a material's ability to generate usable power from a given fuel volume. Terrestrial demonstrations have shown that the highest burnups in test reactors have come from $UC_{0.5}O_{1.5}$, and are as high as 19% [8]. Although terrestrial in application, this performance study of an HTGR and TRISO geometry demonstrates their superiority in high-burnup environments. Since the core's reactivity (and energy output) is not critically dependent on the fissile material, the following sections compare some of the benefits and drawbacks of individual fuel types.

2.1.1 Uranium Dioxide

Uranium dioxide was adopted as the conventional nuclear fuel early in the nuclear energy era as a replacement for uranium metal. It is currently being used in over 90% of commercial power reactors worldwide, and has an impressive set of data covering LEU's performance as a nuclear fuel. UO_2 has a long track record of reliability, and the mechanisms to reduce the risk of failure in the fuel are well-understood. However, there are several drawbacks to UO_2, especially concerning powering a TRISO-based reactor in space.

The thermal conductivity of uranium dioxide is comparatively very low. Fuel additives that increase net thermal conductivity have been tested for use as a base for accident tolerant fuels (ATFs). For example, NASA's KRUSTY was built around a 7% molybdenum fuel [4]. Many of these additives to UO_2 are fairly novel propositions, and adapting them for use in space may prove to be time-intensive and costly. Furthermore, the addition of other compounds in nuclear fuels reduces the uranium loading and, therefore, decreases the overall reactivity. UO_2 exhibits a higher fission rate with temperature, and the targeted burnup of a UO_2 fuel kernel is relatively high.

Several unique modes of failure have been observed in uranium dioxide-based TRISO fuel particles. UO_2 experiences uranium-oxygen debonding at high operating temperatures, which produces CO_2 and CO. These contribute to internal pressure on the iPyC layer and can lead to cracking or layer debonding. These have historically been mitigated by including a thick buffer layer without the kernel. For the purposes of core mass reduction, this essentially equates to

unused space and mass. Other modes of failure have been recognized in UO_2-based TRISO fuels, including kernel migration, fission product chemical attack on the SiC layer, yielding of the SiC layer, chemical debonding between the layers, and thermal decomposition [11].

2.1.2 Uranium Carbides

UC_X was considered and tested early in TRISO particle development. The introduction of uranium carbides to HTGR fuel has mitigated many of the irradiation-induced modes of failure within oxygen-centered TRISO kernels. As shown in Figure 2.1, UC exhibits a significantly higher thermal conductivity than UO_2. Use of strictly UC_X is not without drawbacks, as free oxygen from UO_2 reactions oxidizes fission products which prevents them from critically damaging the SiC layer [12][28].

Most research into uranium carbide fuels prefer to combine UC_X with uranium dioxide, creating a fuel type that is commonly referred to as uranium oxycarbide (UCO), or specifically $U(O_2,C_X)$. Typically, the stoichiometry of the UC_X phase is UC_2, although any stoichiometry would effectively mitigate the production of CO and CO_2 in the particle [28]. Since both UO_2 and UC_2 provide performance improvements, studies tend to focus on the balance between the two molecules. The limitation of oxygen production within the fuel is associated with decreased pressure and kernel fuel migration, meaning an increased kernel size is conceivable.

In the US, UCO is the foremost contender for future Gen-IV HTGR fuel. For example, INL's ATR has been running primarily on UCO fuel. The fuel is typically close to a 3:1 ratio of UO_2 to UC_2 [26][29]. This convention is descriptive of the ratio identified in many studies, specifically that no more than around 5-6% UC_2 at% is needed to offset CO and CO_2 production from UO_2 [28].

2.1.3 Uranium Nitrides

Uranium nitrides are gaining favor as a potential replacement for uranium dioxide across the nuclear industry. UN has a much higher thermal conductivity than UO_2 (Figure 2.1), creating a more even temperature distribution within a TRISO particle and pebble, leading to an improved

overall thermal efficiency of a reactor core. For use in HTGRs, the decomposition of UN_X to UN means that UN specifically is the only potential candidate material for TRISO kernels in this study [27]. UN has a slightly higher uranium loading, which improves the core reactivity. Studies have shown that it yields up to 40% more uranium than in UO_2, which greatly increases burnup [35]. Uranium mononitride has a longer fuel cycle than what is seen in traditional commercial environments [35]. It has a melting point that is comparable to uranium dioxide and is far higher than what is necessary for HTGR operation ($\sim$1300 C). Like UC_X, uranium nitride does not produce CO or CO_2, which reduces the necessary volume of the buffer layer [30]. One study in particular shows promise for using UN as a TRISO kernel with significant reduction to core mass and size by increasing the size of the particle kernel itself [30]. A mixture of uranium carbide and nitride fuels has also been investigated and is intended to combine the benefits of both [13].

There are some associated drawbacks to UN, however. The production of uranium nitride as a fuel is a complicated process. Furthermore, not much data exists for UN, let alone for specific use in space nuclear reactors, HTGRs, TRISO geometries, or the lunar environment. This would make it difficult to seriously consider as a candidate for the Artemis Program. It also restricts the oxidation of metal fission fragments that could damage the SiC layer of the particle.

2.2 Graphite Layer Manipulation

Two methods of particle layer manipulation were undertaken in an effort to minimize the mass required to achieve criticality. These included both varying the materials used in the layers of a TRISO particle, and changing the radial thicknesses of the layers. Concepts to remove layers altogether from a TRISO particle were investigated, which essentially yielded what is referred to as a bistructural-isotropic (BISO) fuel particle. This idea, however, did not garner serious consideration since BISO particles (or any particles with fewer structural and protective layers) cannot be used in as high of temperature or burnup conditions [20]. This makes them significantly less ideal for extraterrestrial applications.

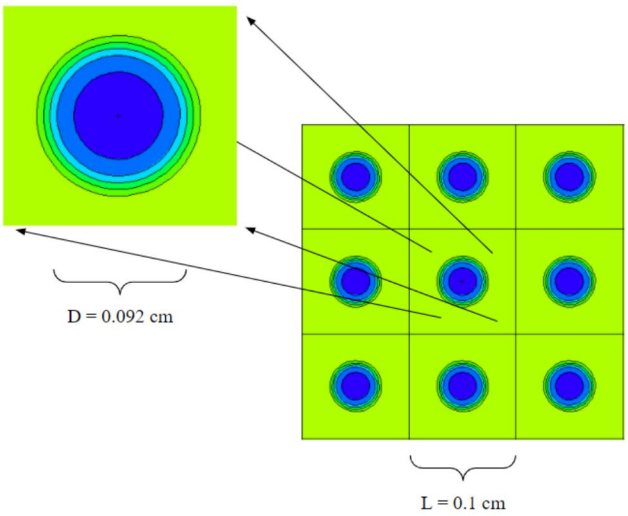

Figure 2.2: A 2D cross-section of TRISO particles embedded in a graphite matrix to be used in a core assembly

While making these variations, the mesh size (pitch) of the core matrix model itself was left constant. Figure 2.2 shows a 2D cut-out of the particles embedded in a pebble within the core.

2.2.1 Layer Thickness

Table 2.3: Properties of TRISO particle layers and sample particle layer dimensions [26]

Material	**Thickness (μm)**	**Density (g/cm^3)**	**Thermal Conductivity at Operation (W/mK)**
Fissile Kernel	250 (radius)	-	-
Porous Carbon Buffer	100	1.0 (50% porosity)	0.5
Pyrolytic Carbon (iPyC)	35	1.9	4.0
Structural Layer (SiC)	35	3.2	30.0
Pyrolytic Carbon (oPyC)	40	1.9	4.0

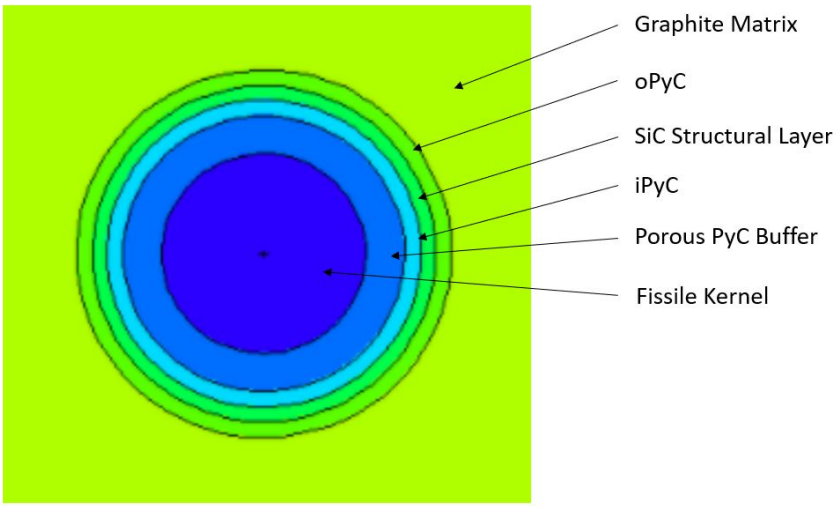

Figure 2.3: Image of a TRISO particle cross-section from the MCNP core model

As alluded to in the introduction, a TRISO particle consists of several structural and performance-enhancing layers outside of the fissile fuel kernel. Typically, a porous, low-density buffer layer directly encases the kernel. This buffer mitigates many of the early symptoms of possible kernel failure and helps contain fission products. UO_2 notably creates CO, which causes pressure buildup within a particle. The pressure induced on the inner walls of the TRISO layers is mitigated by the porosity of this buffer layer.

An inner pyrolytic carbon (iPyC) layer exists immediately without the porous buffer. It acts as another fission product shield and supports the proceeding SiC structural layer. This SiC layer provides most of the structural support to the particles and is designed to be robust under high temperatures and irradiation. Lastly, the outer layer of pyrolytic carbon (oPyC), contributes to the structural integrity of the SiC later. It also acts as a protection to the other layers.

A TRISO particle model with labelled dimensions is shown as Figure 2.3 and Table 2.3. Although these dimensions represent what is most commonly used in test reactors in the United States, these dimensions are specifically taken from a thermal study conducted by Los Alamos National Lab (LANL) [26]. Several variations to this traditional model have been examined. These

variations use the 3:1 ratio of UO_2 to UC_2 (denoted $UC0.50_{1.5}$) at 20% U-235 enrichment, unless otherwise specified.

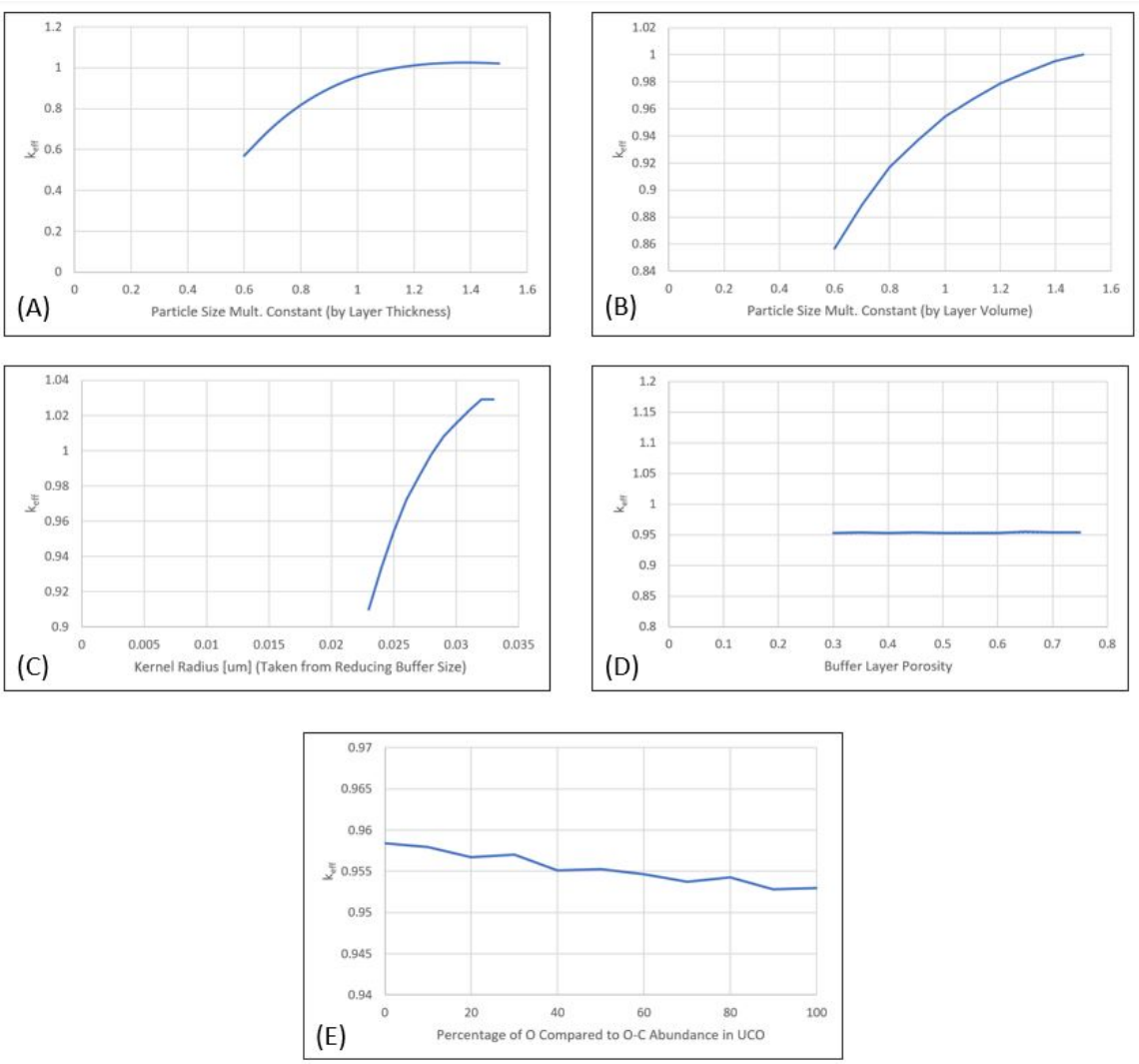

Figure 2.4: Plots with various TRISO particle dimensions

In Figure 2.4, (A) and (B) show how particle size increases overall reactivity in a core. These two plots present similar data, although (A) increases the layer thicknesses by a multiplied constant, while (B) increases the layer volume by the constant. (C) shows that buffer decrease has the same effect on reactivity, or specifically that the increase in the kernel radius at the expense of

the buffer allows for higher achieved reactivity. This is considered because the buffer's function is largely dependent on the oxygen produced, which itself is dependent on the fuel type. (D) shows that there is little to no reactivity change corresponding to buffer porosity adjustments, and (E) shows that there is only a slight change in reactivity by adding oxygen at the expense of carbon in UCO. Exact dimensions of the particle layers are provided in the appendix (Tables A.1-5). Results seem to agree with the expectation that more fissile material has the greatest effect on overall core reactivity.

2.2.2 Layer Materials

There are not many models or experimental studies that consider using materials other than what is convention for TRISO particles. Graphite tends to be commonly used in nuclear fuel because of its high melting point and good neutron moderation. All TRISO particle models use graphite as a matrix material within a pebble. Furthermore, essentially all TRISO studies assume pyrolytic carbon to constitute the protective layers.

There have been several materials proposed to act as a replacement for the structural silicon carbide layer, however. These materials include various other carbides and nitrides, including titanium carbide/nitride, and zirconium carbide/nitride [14]. A study conducted by A. Nosek et al. concludes that a combination of UN fuel and a ZrC structural layer yield's the lowest overall tensile stress in operation (given similar failure stress conditions), although the SiC model consistently performed well in high-stress environments [14]. These model variations were performed on BISO particles, and since the structural layer has little effect on overall core reactivity (and therefore little benefit to mass reduction - see Table 3.1), the lack of experimental data prohibits the realistic use of anything but SiC in an engineered lunar reactor by the 2027 deadline.

Table 2.4: The differences in modeled reactivity between the proposed alternatives for SiC

Material	**Density (g/cm^3)**	**Keff**	**Error**	**Reactivity**
SiC	3.21	0.95415	0.00065	-0.04805
ZrC	6.73	0.95356	0.00065	-0.0487
ZrN	7.09	0.93542	0.00045	-0.06904
TiC	4.93	0.8876	0.00042	-0.12663
TiN	5.40	0.86209	0.00041	-0.15997

3. FUEL ASSEMBLY

3.1 TRISO Fuel Assemblies

This section will examine the simulation and testing required to examine the effects of enrichment on the design of an HTGR reactor. The majority of scientific testing was conducted in MCNP6.2, which was used to design and run a novel HALEU reactor. The section consists of the TRISO reactor design process, with justification, and concludes with the final reactor design used to simulate novel approaches to reducing reactor mass.

3.1.1 Pebbles vs. Prisms

TRISO particles belong to a nuclear fuel element group of coated uranium fuel sources. Since the original coated fuel element was hypothesized in 1957 by R. Huddle [20], coated uranium fuel elements have been devised and tested extensively. TRISO particles are the result of an enormous amount of fuels testing and modulation. These particles are classified in two distinct fuel element groups: pebbles and prisms [20].

As the name suggests, prismatic TRISO fuel elements consist of TRISO particles formed into a fuel element (typically a cylinder) which can be placed into an assembly similar to a fuel rod in pressurized water reactor (PWR) designs. Typically, prismatic fuel assemblies are built from a graphite fuel assembly with TRISO particle pellets placed within the prismatic assembly. Alternatives to the Gen-III fuel assembly design consist of reactors with prismatic TRISO plates placed within graphite plates. The versatility of prismatic designs can lead to limitless reactor core configurations, and is the basis for the low enriched reactor design under study.

TRISO pebbles differ from the prismatic designs by encompassing the TRISO fuel region within an enclosed sphere. Each TRISO pebble is designed to contain roughly 9,000 to 18,000 particles, with an average of 12,000 particles per pebble [11]. Instead of a graphite assembly (as used in a prismatic system) a TRISO pebble is an entirely self-contained fuel element, with an outer coating of graphite around the TRISO particle sphere within. The design of the TRISO pebble

can be seen in Figure 3.1, along with the simulated pebble within MCNP6.2. While a typical TRISO pebble consists of a carbon layer of 0.5 cm thickness surrounding the fuel sphere, this layer was decreased to 0.25 cm in order to increase fuel density at the cost of pebble consistency. Additionally, in early runs, the high neutron moderation present in the reactor supported this design decision as less carbon was needed for moderation.

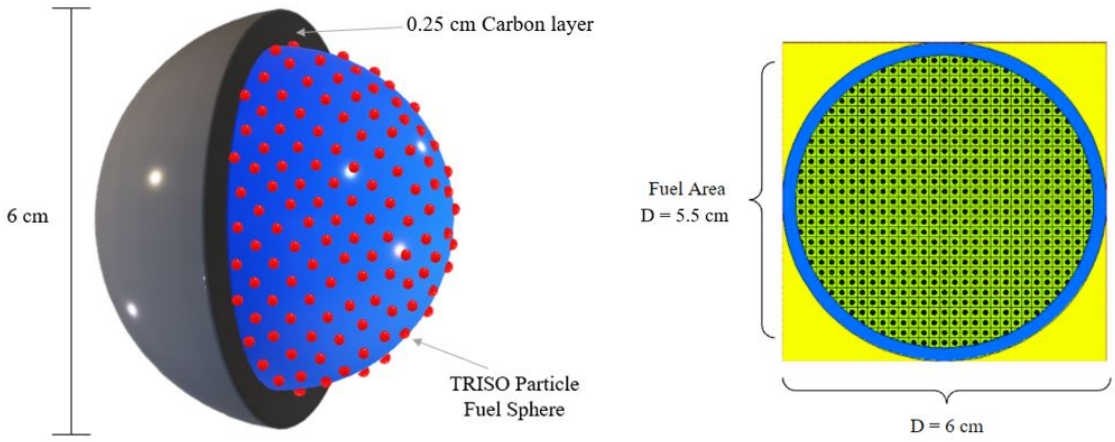

Figure 3.1: TRISO pebble graphic (left) and as modelled in MCNP (right)

TRISO pebbles are usually found in pebble-bed style reactors and have different loading procedures and safety tolerances than typical Gen-III core designs. The fuel element is self-contained and enclosed in graphite, therefore this fuel design has increased accident tolerance features, among other favorable characteristics for use in space.

For the purpose of this design optimization task, the pebble bed reactor design was ultimately chosen to simulate TRISO particles. The choice of pebbles over prisms was a result of the existing pebble designs which could be simulated effectively in MCNP6.2. In this way, the pebble effectiveness of real-world fuel could be measured and altered in order to optimize mass. Addi-

tionally, the passive safety features of TRISO fuels would yield greater accident tolerance features, therefore creating a safer and simpler reactor system. This was viewed as especially favorable as the reactor will need to operate for many years without refueling or fuel shuffling.

Furthermore, the choice of using TRISO pebble fuel elements over prismatic narrows the newly optimized variables within existing TRISO and pebble bed designs. By using a set variable fuel element and a simple HTGR pebble bed, the effects of enrichment, burnup, materials, and geometry of the particle could be compared in a defined system. Having a core which consists of pebbles emphasises the effect of particle changes made during design iteration, where having an undefined amount of geometric prismatic designs would become an overwhelming task to model and compare. Rather than constantly altering the core design with new plate or pellet configurations, choosing a stable pebble based off of real-world production allowed for consistency when attempting to demonstrate particle effects on reactor design. High-density, low mass materials should be used as neutron moderators (graphite) within the particle assemblies, and the coolant itself should be a low-mass neutron energy absorber.

3.2 Pebble Bed Arrangement

The arrangement of the TRISO pebble bed contributes to the overall mass of the reactor core. The chosen stacking method of the TRISO pebbles will vary the density of the fuel arrangement. The chosen coolant (usually helium) freely flows between TRISO pebbles through the reactor core. Typical TRISO pebble bed reactors are designed to allow for pebble loading through the top of the core and removal from the bottom. This system cycles the pebbles throughout the reactor core. X-energy, a company currently producing Gen-IV reactors, has a design which refuels new TRISO pebbles daily, removing spent pebbles from the bottom and recirculating the pebbles up to six times for a maximum commercial fuel lifetime of about three years [25].

Pebble arrangement for this study was determined through two types of sphere-packing methods. There are numerous sphere-packing methods, however the chosen model simulated pebble spheres with the highest packing-density within a cubic cell [24]. This packing model, hereby referred to as “method 1”, is shown in Figure 3.2, along with the alternative packing model, de-

noted as “method 2”. Sphere packing density can be given by Eq. 1, which shows the relationship between sphere side length and minimal separation between spheres.

$$L = 2 - \frac{2}{d_n} \qquad \text{(Eq. 1)}$$

Where L is the side length and d_n is the greatest minimal separation between points.

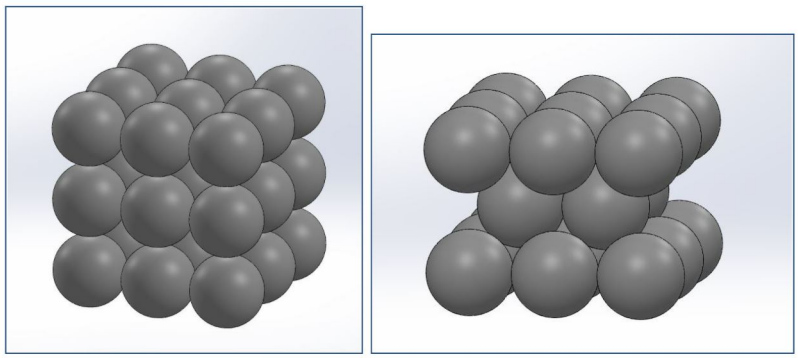

Figure 3.2: Packing method 1 (left) and packing method 2 (right)

Table 3.1: Comparison between packing methods and volumetric ratios

Packing Method	**Density**	**Spheres in Cube**	**Length (cm)**	**Volumetric Ratio Sphere/Cube**
Method 1	0.25	27	18	0.5235987755
Method 2	0.215	14	14.48528356	0.5209540339

The volume of a cube to a sphere yields a packing ratio of 0.5236, as seen in Table 3.1. Method 1 was chosen as it has the densest configuration. With the assumption that greater fuel density leads to a greater multiplication factor, both methods were modeled to find the effect of pebble density (with a helium coolant) on the overall effective multiplication factor. In a completed core model, the highest density packing method, method 1, yielded a multiplication factor

of $1.14718 \pm 5.28 \times 10^{-4}$. Method 2's packing density yielded $1.12921 \pm 5.08 \times 10^{-4}$. This gives a difference in multiplication factor of $0.01797 \pm 7.326 \times 10^{-4}$. Since criticality must be sustained, the highest density packing method was chosen to simulate the TRISO pebble bed arrangement. Although there may be inaccuracies in simulation, real world pebbles are expected to shift or sit imperfectly. Here, the densest configuration allowed the smallest theoretical critical mass to be obtained. In order to simulate the spheres in MCNP, coordinate positions were identified within the sphere and altered to fit cube dimensions [23].

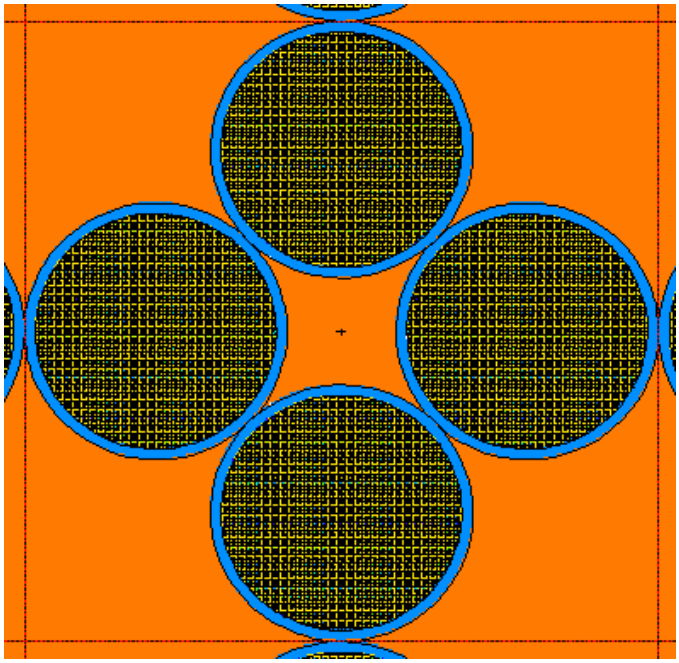

Figure 3.3: Alternative pebble stacking method 2 in MCNP

3.3 Core Design and Simulation Methodology

With the core design established as a pebble bed reactor with the method 1 packing assembly, the MCNP6.2 model could be written and used to assist in the design process. First, the particle was designed using a typical TRISO particle layer thickness. Figure 2.2 shows the original particle geometry as simulated in MCNP. The particle consisted of a uranium metal kernel with

Table 3.2: Base TRISO particle dimensions

Element (From Center - Out)	**Diameter (cm)**
U Kernel	0.05
Porous Carbon	0.069
Inner Pyrolytic Carbon	0.077
Silicon Carbide	0.084
Outer Pyrolytic Carbon	0.092

20 wt% enrichment. Table 3.2 contains the particle material and dimensions of the initial TRISO particle simulated.

As seen in Figure 2.2, the particles were simulated in a grid of repeated universe cells. This grid encompassed the 3D spherical fuel region within a TRISO pebble, as shown in Figure 3.1. The TRISO pebble was simulated with a 3 cm radius and a 0.5 cm-thick layer of carbon which encased the fuel region. Due to the low enrichment of the pebble and lack of high uranium density, attempts to simulate a single pebble yielded very sub-critical multiplication factors (< 0.1). This was expected, and in order to find the critical configuration required, the reactor core needed to be simulated in its entirety.

The reactor core design was based off of a previous TRISO fueled design using high enriched uranium at 95 wt% U-235 [24]. The general shape of the reactor was used, and the fuel elements were replaced with a pebble bed design. The core began as a simple cylinder enclosing a pebble cylinder stack. From there, the core dimensions were varied to approach a multiplication factor of 1. The design iteration process was recorded in Table A.6. The initial goal of the process was to find a critical reactor core configuration. In order to compare the TRISO pebble reactor results to the modelled highly enriched prismatic reactor design, the ratio of the design was used to determine the fuel element height-to-radius ratio, the containment vessel thickness, etc. The reactor dimensions were iteratively altered based off of output in order to converge to the smallest possible reactor which could maintain criticality.

Once the critical configuration was found, the next step was to add reflectors to the reactor core in order to shrink the overall size and mass of the fuel region, as well as introduce control to

the reactor core. This consisted of control columns which were inserted axially into the reflector. These columns were composed of beryllium oxide (BeO) as the reflector material, except for a portion which contained boron-10. This portion formed a half circle slice in the control column which, when rotated, acted as a method to increase and decrease neutrons in the core. Additionally, a control channel was added in the center of the reactor core in order to mitigate safety concerns for an accidental water landing. In the event of a water landing, the control channel (which is normally filled with He), is flooded with boron-10. This is a response from a control rod which is placed above the reactor core which is only used in emergency situations, and is intended to significantly increase negative reactivity, thereby negating the increased moderation that sea water would introduce. Both the control channel and the thickness of the control column absorbers were altered based on design output and criticality simulations, and a general reactor design was obtained (Figure 3.4).

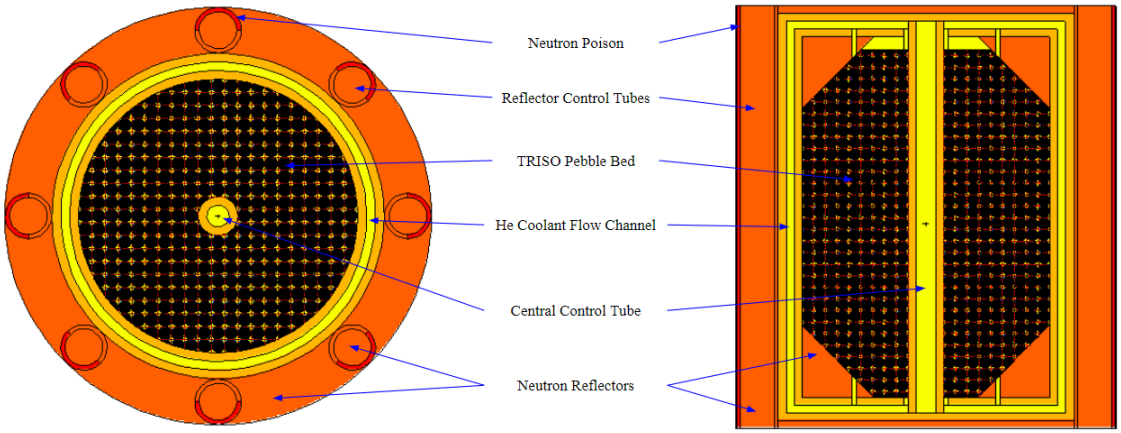

Figure 3.4: Initial pebble bed reactor design simulated in MCNP

The initial pebble bed reactor design was determined based on similarity to the modelled reactor design, as well as output from MCNP criticality calculations. The multiplication factor of the reactor at full power is $1.01960 \pm 4.49 \times 10^{-4}$ and $1.01712 \pm 4.68 \times 10^{-4}$ when at minimal power.

3.4 Final Core Design and Simulation

The final reactor design expanded the initial design by adding eight additional control drums. Initial runs with the final reactor design showed limited control with drum rotation. The initial reactor model was used to understand the physics of reactivity feedback as the particle design varied. Final simulation also included reactor burnup runs, neutron flux in the fuel kernel, and dosage calculations at 100 m from the reactor core. Additionally, a 234-cm lunar surface depth was added to model the effect of neutron scattering on regolith. The composition of the lunar regolith was determined through analysis of previous atomic compositions measured and recorded in other research publications [22]. The final reactor design, with focus on individual component dimensions, is represented in the following figures.

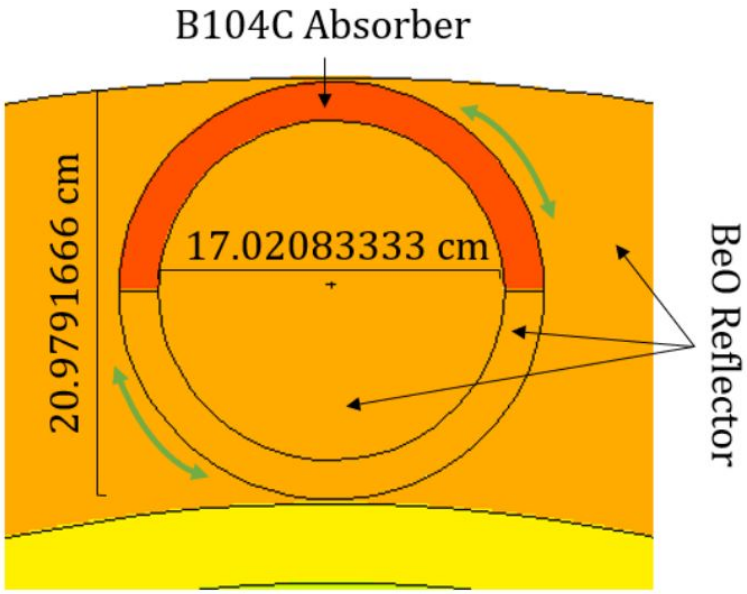

Figure 3.5: View of a control drum configuration and dimensions. The drum is able to rotate in either direction,thereby changing the orientation of the ^{10}B absorber (shown in red)

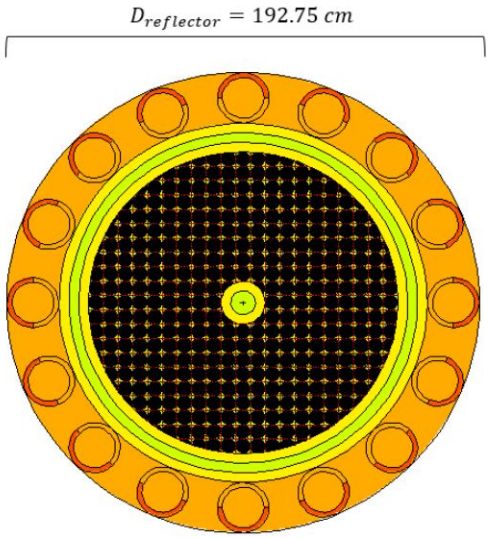

Figure 3.6: Cross-section of the center of the reactor through the total diameter

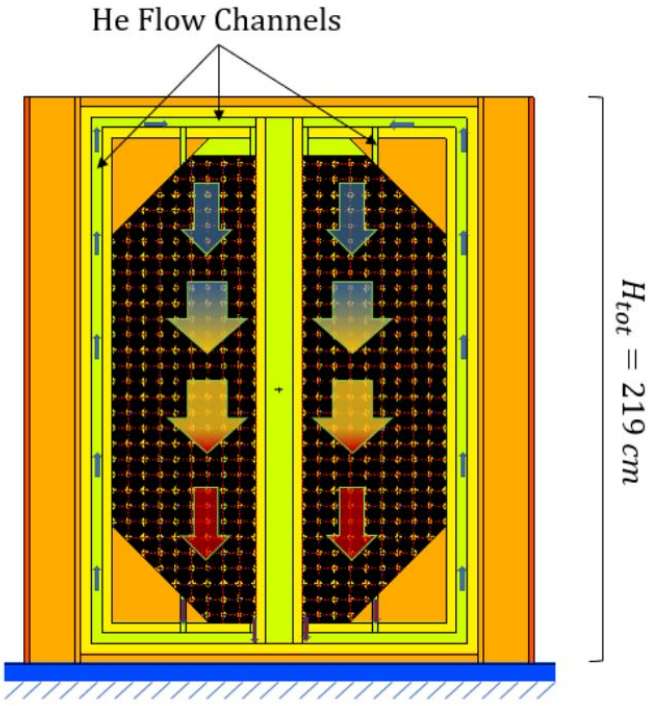

Figure 3.7: Cross section of the center of the reactor with arrows to show a potential path for He coolant flow through the core and He flow channels. Direction of the He flow would depend on the power conversion system placement

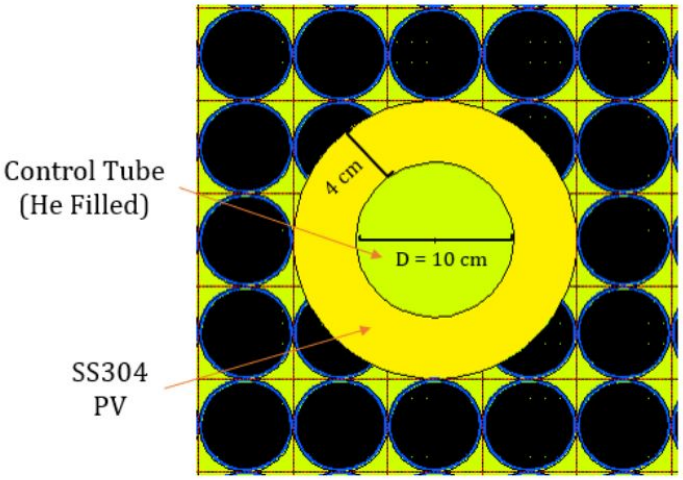

Figure 3.8: Cross section of the central control tube used for emergency negative-reactivity injection

4. CORE CHARACTERISTICS AND POWER IMPLICATIONS

4.1 Power Conversion Systems for HTGRs

There is a direct proportionality between the neutron flux and the thermal power used, therefore heat rate produced in the reactor core can be understood in terms of the fission reaction rate. Furthermore, the heat flux determines the reactor outlet temperature, which contributes to the cycle efficiency. Determining a power cycle is necessary in order to convert heat input into mechanical work output as effectively as possible. Both Brayton and Stirling cycles were considered for use in the space reactor design. Both thermodynamic cycles are heat engines, which means they transfer heat from low to high temperatures. In general, the larger this difference in temperature, the more efficient the cycle. Rankine was not considered because it incorporates two-phase fluid flow, which is difficult to manage in a low gravity environment [16]. Additionally, static conversion technologies like thermoelectrics and thermionics were not considered. Although they are older technologies that are proven and lower risk, the performance, efficiency, and lifetimes of these systems discount them from further analysis [16].

In a low pressure, low gravity lunar environment, the thermodynamic cycles to be examined were narrowed to Stirling and Brayton, since they both use single-phase fluids throughout the cycle. A two-phase fluid system introduces more complexity in the low-gravity environment. One of the most important metrics for selection of the cycle is efficiency. Through efficiency, the physical size and mass of the nuclear heat source can be further optimized. Furthermore, a more efficient cycle increases the quality of the waste heat, which can assist in the heat removal process - another topic which garners further exploration.

It should also be noted that the power performance will also influence the mass constraints. The mass of the design scales up with power. Previous studies conducted by NASA show that Stirling power conversion provides a 14% mass benefit at a power level at 10 kW [16]. This led to the decision of selecting Stirling as the optimum power conversion cycle.

4.1.1 Brayton Cycle

A Brayton cycle describes the process of a constant pressure heat engine. The entire cycle undergoes four processes - two isentropic processes and two isobaric processes. It does not execute isothermal processes, as these must be conducted slowly. There are two types of Brayton cycles - open and closed.

The open cycle takes ambient atmosphere and compresses it to a higher pressure and temperature. The air is heated in a combustion chamber via the burning of the fuel-air mixture. The product gases are then expanded in the turbine, which produces mechanical energy. Generally, the Brayton cycle will discharge gases directly to the atmosphere of the outer system. An open system is not an option for this project, as the reactor chamber should not be open to the low pressure environment [19]. The closed Brayton cycle recirculates the working fluid (the coolant). The gas which is expelled from the turbine is recycled back into the compressor. This cycle is typically used for high temperature gas cooled reactors, and would be the cycle selected for our design if Brayton were to be incorporated into the reactor design. The Brayton cycle has the advantage of technological development and utilization since the 1960s [19].

4.1.2 Sterling Cycle

The Stirling cycle is a closed regenerating cycle which also uses a gaseous working fluid. It typically uses a piston to displace heat between a heated and unheated cylinder. However, in order to reduce system complexity and increase the overall service lifetime, there was a push for development of free piston Stirling technology from NASA in the 1980's with the SP-100 Space Reactor Program [16]. The data from these experiments show that the efficiency of piston-free Stirling technology is one of the highest recorded. The free piston Stirling engine is a dynamic converter which has been widely used due to its high efficiency and reliability [10][16].

Note that the maximum power output of this thermodynamic cycle is not simply a function of the temperature difference between the hot and cold processes. Rather, it is also a product of the maximum allowable stroke of the piston, which displaces the coolant between the heated and

unheated cylinder. The stroke length of the piston produces a voltage based on the frequency; to increase the power, voltage and stroke must be increased. This is limited by geometry of the design. Further optimization of the Stirling heat engine must cover the length and diameters of the displacement cylinders, the piston displacement, and the length of the stroke, among other constraints. This is beyond the scope of the current study.

Previous research in comparison studies of Brayton vs. Stirling cycles for space applications show that different cycles should be utilized according to the power-output to mass savings. Brayton cycles achieve "40% of Carnot at cycle temperature ratios between 3 and 4, while free-piston Stirling machines can achieve 60% of Carnot at temperature ratios between 2 and 3" [19].

The characterization of this core design and its power output will be examined through a Stirling thermodynamic cycle. The cycle's efficiency, and use in past space energy systems, makes for an appropriate choice for a small reactor with a small required power output.

4.1.3 Helium as a Coolant

Helium was ultimately selected as the coolant candidate due to its low viscosity, low density, and high thermal conductivity at the supercritical state. These properties are listed in Table 4.1. The working fluid will be a supercritical state throughout the power cycle. The average operating pressure of the cycle was 144.3 bar, or 14.5 MPa. This, and other features of the Stirling cycle, are discussed further in Section 4.2.2. Alternative cooling cycles, such as nitrogen or other disassociating gases, were not considered.

Table 4.1: Helium thermophysical properties at supercritical conditions [38]

Temperature (K)	**Density (g/cm^3)**	**Thermal Conductivity (MW/cm-K)**	**Viscosity (g/cm-s)**
300	2.20E-02	3.82	2.04E-04
1200	9.93E-03	4.11	5.27E-04

4.2 Power and Efficiency

4.2.1 Thermal Design Limits

SiC and graphite are used to contain fission products within the TRISO particles, and therefore assist with the thermal design limits. Since the release of fission products is dependent on temperature, the steady state thermal limit is set at 1573.15 K, and 1873.15 K at peak transient [17]. The fuel centerline temperatures are set to reach a maximum temperature of 1200 K, which is well-below this thermal design limit. Any other imposed thermal limitations would be for the benefit of the reactor pressure vessel, reflector, and control rod materials (there was no cladding to consider) [17].

4.2.2 Volumetric Heat Generation and Power Density

Examination of the fission reaction rate is necessary to find the volumetric heat generation rate. Eq. 1 below was used to estimate the needed neutron flux in order to generate 10 kW of power. After a core configuration was found, Eq. 1 was also used to determine the volumetric heat generation rate produced by the fuel kernels. In this sense, the equation is a measurement of the heat generated per unit volume of the fuel within the core.

$$\phi(r) = \frac{q'''(r)}{\chi_f \sigma_f^{235} N^{235}} \qquad \text{(Eq. 1)}$$

The volumetric heat generation rate was then included in Eq. 2, where core power density (Q"') was calculated. Power density is a parameter commonly used as a figure of merit measuring the core's thermal performance. Since the size and mass of this reactor must be minimized, the power density figure is critically important.

$$Q''' = \frac{Q'_{th}}{V_{core}} \left(\frac{kW}{L} \right) \qquad \text{(Eq. 2)}$$

Table 4.2: Power density, volumetric heat generation and core dimensions [15]

Reactor Radius (cm)	75
Reactor Height (cm)	211
Reactor Volume (L)	3728.677781
Avg. Flux (n cm^2)	8.67×10^{10}
Volumetric Heat Generation (kW)	47.2705
Power Density (kW/L)	0.0211

Mass, volumetric heat generation, and power density were calculated for several reactor variations, with the characteristics of the final reactor configuration in the table above. The calculations were conducted with a Matlab model, which held the following constants:

- Enrichment was constant at 20%.
- The number of fuel particles per pebble was held constant at 12770, based on the average number of particles in the MCNP model.
- The number of pebbles in the core was held constant at 11,176, based on the average number of pebbles in the MCNP model.

Additional calculations included generating a time stepped temperature distribution of the heat flux and temperature across a typical TRISO particle. A centerline fuel temperature of 1300 C was assumed, based on typical values for steady state 100% power [17]. Note that this is within the thermal design limits outlined in Section 4.2.1. It was also assumed that the coolant passed directly over the TRISO particle. These calculations led to the surface temperature of the particle reaching 1200 K.

Table 4.3: Design parameters of a Stirling power cycle

Hot End Temp (T_H)	1200 K
Cold End Temp (T_C)	300 K
Compression Ratio	2
Volume of He at State 1	2.56×10^6 cm^3
Predicted Frequency	0.09933 RPM
Predicted Power Out	35.25 kW
Predicted Efficiency	0.75
Predicted Average Pressure	1.443×10^4 kPa
Swept Volume	1.28×10^6 cm^3
Mass of Working Fluid	1.643×10^7 mg
Work Out Per Cycle	2.129×10^7 J
Predicted Specific Work Out Per Cycle	1.296 (J/mg-working fluid)
Temperature at State 1	300 K
Volume at State 2	1.280×10^6 cm^3
Temperature at State 2	300 K
Volume at State 3	1.280×10^6 cm^3
Temperature at State 3	1200 K
Volume at State 4	2.560×10^6 cm^3
Temperature at State 4	1200 K

The parameters generated in Table 4.3 were calculated with helium as the working fluid and with a few additional assumptions:

- Both the compression and expansion processes are adiabatic.
- There is no pressure drop or gas leakage throughout the cycle.

- The temperatures in the heater and cooler were constant.
- The regenerator operates as an ideal system.
- The working gas is an ideal gas.

For the purposes of this project, the ideal Stirling analysis was sufficient to confirm that the reactor could successfully operate to its desired work output. The predicted efficiency reaches 0.75, which will decrease with further exploration into the experiment evidence. The next steps in this process should include heat loss analysis through experimental work. A design of a Stirling engine should be modeled and evaluated, since the engine characteristics will influence the heat loss of the system. Other characteristics listed in the table above, such as the swept volume and predicted piston efficiency, will assist in the future design of a Stirling engine for this reactor core.

It should be noted that the thickness of the pressure shell heavily influences the efficiency of the system, since heat conduction contributes greatly to the overall heat loss. The thickness of the current pressure vessel design is 4 cm. While this could be considered thin already, the pressure vessel is also one of the heaviest parts of the reactor, and the minimization of its mass should be further investigated. The regenerator efficiency is also a place where heat loss will need to be examined and minimized.

A free-piston Stirling engine for space is typically operated from between 5-15 MPa [37]. With this in mind, an average pressure of 14.5 MPa was deemed reasonable for operating conditions.

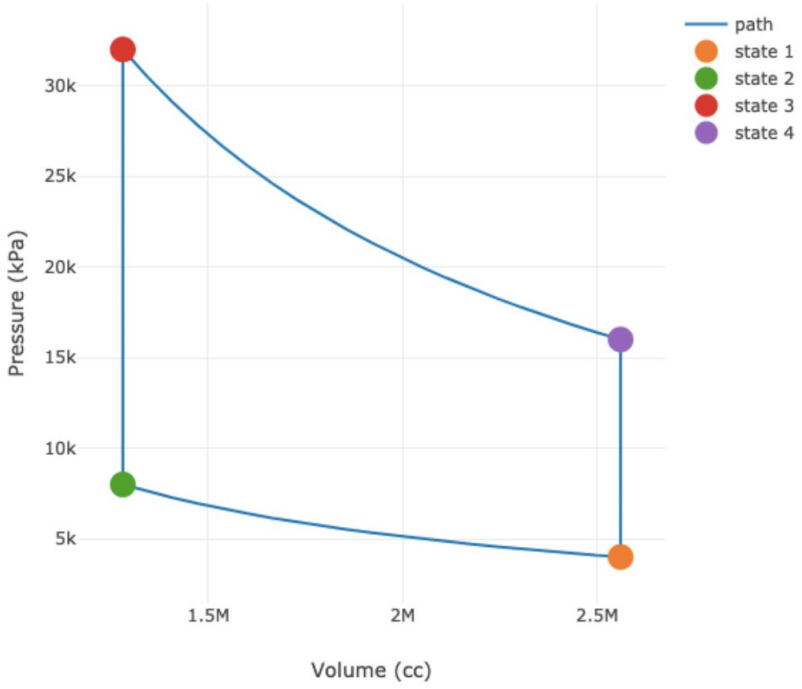

Figure 4.1: P-V diagram for an ideal Stirling cycle

Figure 4.1 shows the ideal Stirling cycle's pressure-volume diagram. The efficiency of this cycle is undoubtedly a higher estimate than can be accomplished in realistic applications. After heat loss has been evaluated, the true efficiency of the cycle can be determined.

4.3 Overall Mass and Design Specifications

The core design was limited by a mass constraint of 3500 kg. This section will examine where the core design meets these specifications, and where it fails.

4.3.1 Fuel Particles, The Pebble-Bed Assembly, and the Overall Core Mass

This study concentrated on the optimization of mass by redesigning a relatively new fuel type - TRISO pebbles. This study has shown that it is possible to create a lightweight nuclear fuel with LEU uranium, and achieve the lifetime and power goals. However, the mass problem cannot be solved by optimizing the fuel alone. As shown in Table 4.4 below, the moderating graphite and the pressure vessel containing the pebble bed contain the majority of the mass of the reactor core.

Table 4.4: Mass and volume dimensions of the materials in the core design

Material	**Volume (m^3)**	**Mass (kg)**
Fuel Particles	0.0582	195.3
Fuel Kernel (U)	0.00934	105.1
Fuel Pebbles	1.26	2820.5
Graphite	0.36	2625.16
SS-304	0.166	7685.5
Helium	2.56	0.46
Total		**13130**

The pressure vessel material was modeled using stainless steel 304 (SS-304), with a thickness of 4 cm for both the inner and outer containment cylinders. The reduction of thickness would increase the heat loss via conduction (and therefore reduce the power system efficiency), and increase the stress exerted on the vessel. Reducing thickness could also reduce the lifetime of the reactor vessel, but it may still achieve the lifetime constraint required. The reflector is not included in Table 4.4. Section 4.3.2 discusses the reflector, and its effects on the neutron economy of the core. Note that the reflector must be included in the design, since it is necessary to bring the reactor to criticality.

4.4 The Reflector

The reflector design is a non-multiplying medium composed of BeO, in the shape of a cylinder, and encases the fuel and graphite matrix. The reflector is necessary to maintain the neutron economy since it scatters many neutrons back into the core and increases k_{eff}. Additionally, the reflector reduces the amount of fuel needed to maintain criticality. The reflector is one of the heaviest objects in the reactor, but it is necessary to increase power and reduce the minimum critical size of the reactor. The maximum size of the reactor is limited by the size of the cargo storage on the rocket transport. The Space Launch System (SLS) Block 2 cargo size is 111.25 m in height

and 8.4 m in diameter, so the reactor sizes examined were within the storage size limits [21].

Table 4.5: Reflector dimensions with mass and k_{eff} output

Variation	**Thickness (cm)**	**Radius (cm)**	**Height (cm)**	**Reflector**	k_{eff}	σ
a	14.88	76.88	89.6	1750.05	0.7	
b	16.8	86.8	101.1	2518.67	0.90020	0.00044
c	16.8	86.8	101.1	2518.67	0.89932	0.00044
d	19.2	99.2	115.6	3759.64	1.02367	0.00046
e	19.95	89.95	101.1	3051.00	0.90031	0.00043
f	19.95	89.95	101.1	3051.00	0.90100	0.00046
g	19.95	89.95	101.1	3051.00	0.90015	0.00045
h	19.95	89.95	175.0	5280.58	0.89941	0.00043
i	19.95	89.95	175.0	5280.58	0.89975	0.00044
j	21.375	96.375	211.0	7308.91	1.0196	0.00044

4.5 Fuel Burnup, Flux Profile, and Dose Calculations

4.5.1 Fuel Burnup

Reactor fuel burnup was analyzed through MCNP in order to determine the effective cycle length of the reactor at the 10 kW power constraint. Burnup calculation was performed for a total period of 11 years, with time steps of varying length in order to observe the effect on reactor multiplication factor, fuel composition, and flux. The ideal burnup calculation can be done through simple neutronics calculations to provide a baseline. For example, taken at an average η = 185 MeV per fission, an estimation of uranium-235 fissions can be calculated using dimensional analysis to be 41.52 g U-235.

Using this fundamental derivation of U-235 fuel spent during the 10 year lifetime, the

burnup of the reactor can be expected to be very low in comparison to a typical terrestrial reactor. Only 41.52 g of U-235 fissioned out of a total fuel volume of 105.18 kg, which shows that the burnup calculation yielded an insignificant decrease in multiplication factor. The mass fissioned (if explicitly considering U-235 fission in the energy production of the reactor) would be 0.0395% the total mass of the fuel kernel over 10 years. Additionally, with a low amount of burnup occurring, the production of actinides and xenon within the reactor core should have a negligible effect on the multiplication factor. Fortunately, the MCNP calculations for burnup provided a more substantial calculation of burnup for the final reactor, using an energy deposition tally, and accounting for nuclide production. Using the output of reactor burnup, the U-235 mass was found over the ten year period.

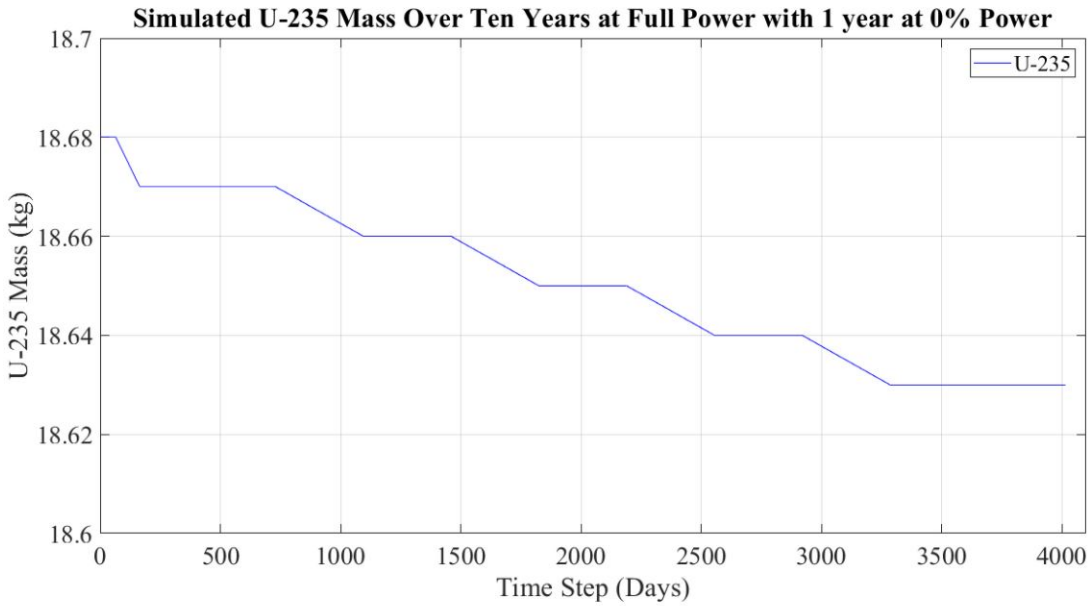

Figure 4.2: Simulated effective multiplication factor over a reactor lifetime of 10 years at full power plotted over burnup

Over the ten year period, the mass of U-235 decreased by 50 g as calculated in MCNP. This difference is more than the ideal value of 41.52 g, but reflects the more complex interactions oc-

curring within the reactor core. Additionally, the range of MCNP nuclide mass is not measured by the gram, and therefore, 50 g falls within a conservative uncertainty range to the ideal. Overall, 50 g is still a relatively small amount of uranium when compared to the total mass of U-235: 18.68 kg at the beginning of life. This resulted in a 2.677% decrease in U-235 mass. Additionally, actinide production within the fuel kernel was relatively insignificant, with a total Pu-239 production of 6.543 g. Additional actinide production was in the milligram range.

4.5.2 Flux Profile

During reactor core criticality analysis, the flux within the fuel kernel of the core was found in order to assist power conversion in calculating the energy transfer to the He coolant. This flux gave an insight into the energy of neutrons being produced and interacting within the fuel area. This directly translates to how uranium fission within the reactor occurs, as fission cross-sections are dependent on neutron energy. Each flux was taken by using a neutron cell tally within all kernels, which tabulated the neutrons track lengths in kernel cells and applied it to the total kernel volume of 9340.84 cm^3. This tally was split into 100,000 energy bins of equal size, from 0 MeV to 30 MeV, in order to observe the spread of neutron flux within the neutron energy spectrum. The output data was plotted in Figure 4.3.

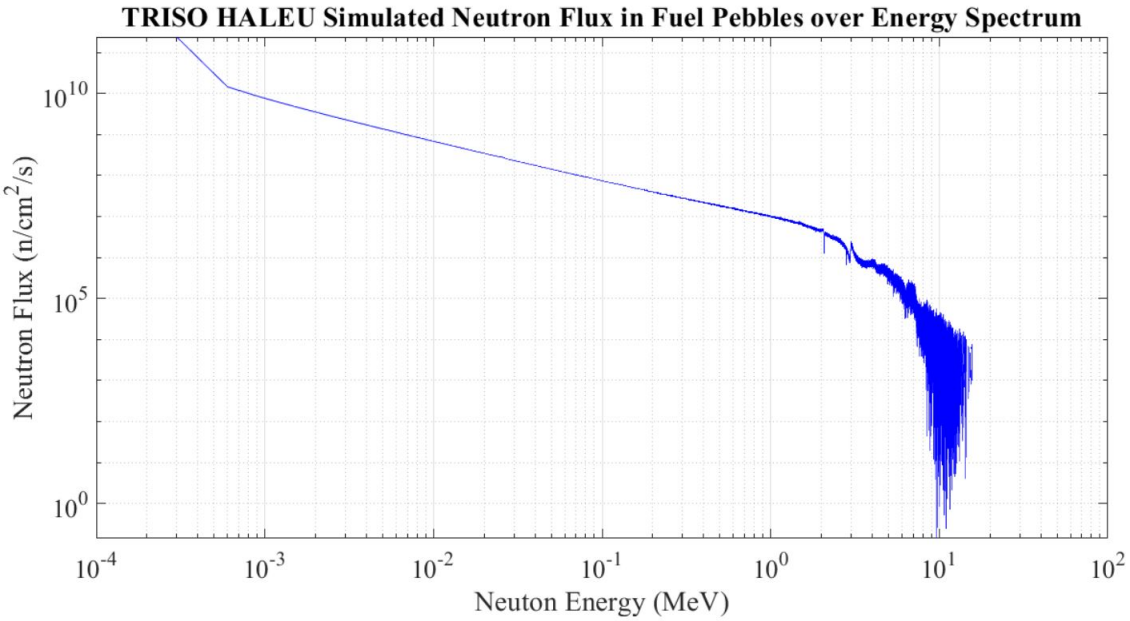

Figure 4.3: The neutron flux averaged within the uranium oxycarbide fuel kernel as affected by neutron energy

When analyzing the neutron flux in Figure 4.3, the first aspect to note is the increase in flux at thermal energies. The linear increase at energies lower than 10^{-3} can be attributed to a very small sample size of flux at these energies, and the true neutron flux at this energy should be decreasing exponentially towards an asymptotic cutoff well above 0 MeV. Due to the limitations of the energy bin calculations, this region was not expected to be accurate. The linear decrease in the neutron flux was an expected effect of the Maxwellian region due to the U-235 cross sections at this energy. Following this distribution, the effects of the U-235 resonance can be seen in the kernel flux in the fast spectrum. Knowing this, it is expected that this reactor operates in the thermal region, and this conclusion was supported by MCNP output, which yielded that average neutron fission occurred at an incident neutron energy of 7.7233 keV, with a ν_f = 2.438 neutrons per fission. The distribution of neutrons causing fission is tabulated in Table 4.6.

Table 4.6: Distribution of neutron energy causing fission

Neutron Energy	**Percent Causing Fission**
>100 keV (Fast)	0.44%
0.625 eV - 100 keV (Intermediate)	8.79%
<0.625 eV (Thermal)	90.76%

4.5.3 Dose Calculation

Dosage for a human sized object at 100 meters on the lunar surface and in a vacuum was also tallied using MCNP. The effective dosage of the human sized target, with atomic composition mimicking that of a human, was found to be $4.139 \times 10^{-14} \pm 7.13 \times 10^{-15}$ Rem/hr. This simulation utilized a human sized slab (x = 30 cm, y = 0.5 cm, z = 175 cm) placed 100 m away from the side of the reactor on the negative x-axis. A diagram of this simulation can be seen in Figure 4.4, with the red object representing the person.

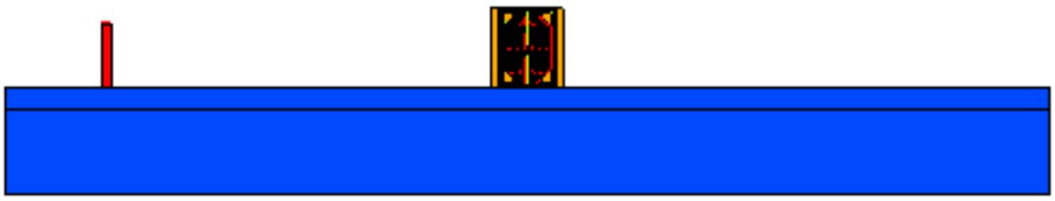

Figure 4.4: MCNP final reactor deck with lunar regolith and a human sized object placed at 100 m from the edge of the reactor core

4.5.4 Effect of Enrichment

In order to thoroughly compare the reactor core to the previous high-enriched designs, the reactor was simulated at different enrichments in order to observe the effect on reactor control and critical mass. The following enrichments, multiplication factors, and criticality control were found.

Table 4.7: Effect of enrichment on multiplication factor

Enrichment (U-235 wt %)	**k_{eff} when at full power**	σ
10	0.92166	0.00043
15	1.01672	0.00046
17.5	1.04756	0.00048
20	1.07241	0.00046
22.5	1.09167	0.00049
25	1.10865	0.00047
35	1.15701	0.00048
45	1.18802	0.00049
60	1.22025	0.00048
75	1.24704	0.00047
90	1.27392	0.00048
95	1.28442	0.00048

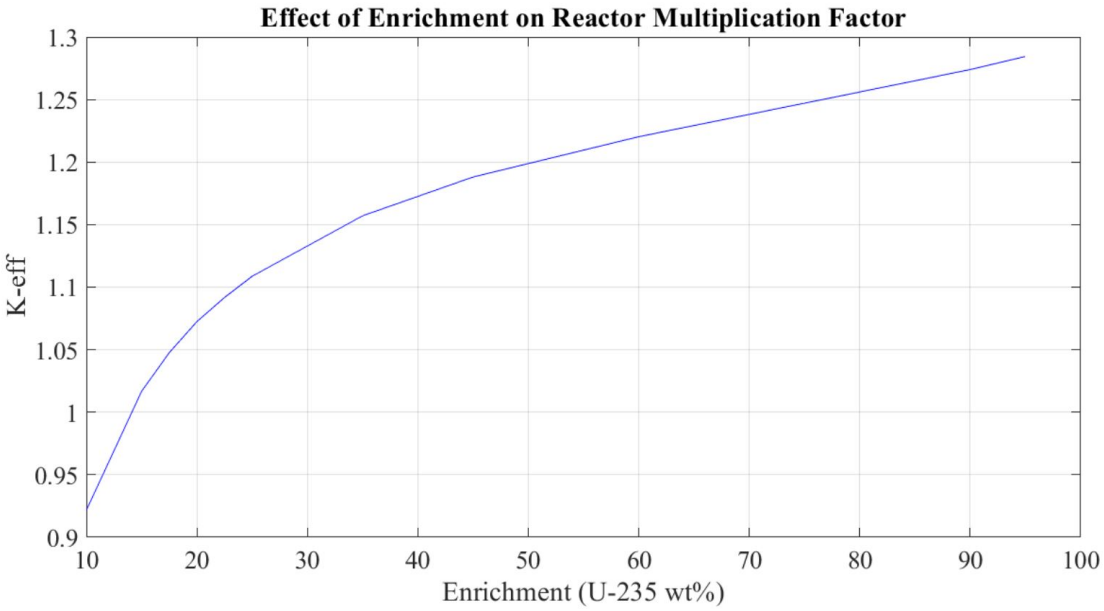

Figure 4.5: Final reactor design with enrichment increasing from 10 to 95 wt%

5. CONCLUSION

When comparing this reactor design to previous high-enriched designs, it is important to recognize the effect that enrichment has on reactor mass and performance. With a higher enrichment, as seen in Table 4.7, the necessary critical mass to achieve criticality will decrease. Burnup results and theoretical calculations yield a similar result, namely that low power output over the course of 10 years is absolutely plausible with a nuclear reactor utilizing TRISO particles at low enrichment. However, there is much more power that can be utilized from a critical reactor of any configuration. Therefore, the power constraint of 10 kW is a very achievable goal.

With a Stirling power cycle, the design requirement of 10 kW is met. The volumetric heat generation in the reactor core reaches $\sim$47 kW. Without a more-detailed design of the power system, including the Stirling engine, associated heat losses within the cycle, and generator efficiency, a definitive power output cannot be exactly computed. However, this estimation meets the design criteria. A Stirling cycle is one of the most efficient cycles today, and is frequently used in space applications. The coolant used in this cycle, helium, has excellent thermodynamic properties in its supercritical state. The mass of the helium is negligible relative to the reactor mass. The coolant will be contained in the reactor system, and recirculated through the entire cycle. The fuel temperatures reached are within the thermal design limits, which was expected with the accident tolerant TRISO fuel.

When considering the design of an extraterrestrial reactor where mass is an ultimate concern, reflectors can be used to increase reactivity without changing enrichment. Unfortunately, reflector mass is considerable in the design of a reactor. A reflector also has limitations - Increasing the reflector will not increase the multiplication factor as the usefulness in reflector thickness follows a normal distribution.

With all parts considered in the design of an extraterrestrial reactor, a higher enrichment would yield a smaller mass profile. The necessary critical radius of the reactor would decrease

substantially, which in turn, decreases the reflector size needed to maintain criticality. The necessary output of 10 kW would be easily achievable either way. At this low power, reactor lifetime ceases to be a figure of merit as it has a low rate of burnup. If nonproliferation concerns are over the production of plutonium in nuclear reactors, then to maintain such a low power would decrease Plutonium production already, as seen by the production of 6.543 g of plutonium in the fuel kernels of this reactor design. If concern exists for the high enrichment of the reactor, a study should be conducted in order to determine the cost of reactor deployment based on the mass of the reactor system (which will be inversely proportional to enrichment).

Specifically centered on the performance of TRISO fuel in an extraterrestrial reactor, there are many benefits to note. First, TRISO fuel could hold an argument for nonproliferation concerns, as the fuel kernel is embedded within the fuel pebble, and would make refinement of actinides difficult. Second, this reactor showed that TRISO fuel embedded within pebbles performed in the thermal region, which has a significant effect on reflector efficiency. Due to the high thermal neutron flux within the kernel, there is evidence that the reactor operates in the over-moderated region. With a majority of neutrons being moderated by the carbon within the TRISO pebbles, the reflector has less effect. There would be a greater amount of fast neutrons in a less moderated fuel type, which would increase the reflector effectiveness and increase reactor control. This consideration should be made when designing a reactor with TRISO pebbles, as the reflector should provide a large source of positive reactivity in order to control the reactor core. Additionally, with the reflector acting as the control, a more efficient reflector would decrease the size necessary to maintain criticality, which would contribute to reducing overall mass.

There are many aspects of this design that could be improved upon in future studies. As seen in the above table, both the reflector and the pressure vessel take up $\sim$60% of the allotted mass. These elements must be further optimized to reduce the overall reactor mass in order to meet the design constraints set out by NASA and the DOE. Further study into the effects of fuel burnup with UCO at higher power should be attempted in real-world experiments, which is a simulation goal that MCNP attempts to replicate. The graphite could also theoretically be reduced,

Table 5.1: Final model mass and volume breakdown

Material	**Volume (m^3)**	**Mass (kg)**	**Mass Percentage**
Fuel Particles	0.0582	195.3	0.0096
Fuel Kernel (U)	0.00934	105.1	0.0051
Fuel Pebbles	1.26	2820.5	0.1380
Graphite	0.36	2625.16	0.1284
SS-304	0.166	7685.5	0.3760
Helium	2.56	0.46	0.00002
Reflector	1.98	7308.91	0.3576
Total	**6.39**	**13131.62**	
Total Mass w/ Reflector		**20440.53**	

since the reactor is operating in the over moderated region. Effects on a reduction in the moderator may prove to affect the reflector efficiency, and improve neutronics and control. And, again, by increasing the allotable enrichment constraint, the mass of the fuel necessary to maintain criticality would decrease.

It is important to note that there are no other low enriched fuels for space applications. In the past, designs and models for space power have utilized highly enriched uranium. It is hoped that the research in this project can provide a benchmark for future mass-optimizations with low proliferation risk and high accident tolerance.

REFERENCES

[1] BATTELLE ENERGY ALLIANCE–DOE CNTR, Bradley, G., Request for Information for Fission Surface Power (FSP) (2020).

[2] Garrett, T. V., BILLING CODE 6450-01-PPosting of the Presidential Policy Directive 6 (Space Policy), "National Strategy for Space Nuclear Power and Propulsion"83923–83927 (2020). Washington D.C.

[3] Mason, L. S., et. al. A small fission power system for NASA planetary science missions (2011). Cleveland, OH; National Aeronautics and Space Administration, Glenn Research Center. NASA/TM - 2011-217099, NETS-2011-3318.

[4] McClure, Patrick R., Poston, David I., Gibson, Marc A., Mason, Lee S., Robinson, R. Chris, 2020. Kilopower Project: The KRUSTY Fission Power Experiment and Potential Missions, Nuclear Technology, 206:sup1, S1-S12, DOI: 10.1080/00295450.2020.1722554.

[5] NASA. (n.d.). Artemis. Artemis: Humanity's Return to the Moon. https://www.nasa.gov/specials/artemis/.

[6] Sondelski, B. and Nellis, G., 2019. Mass optimization of a supercritical CO2 Brayton cycle with a direct cooled nuclear reactor for space surface power. Applied Thermal Engineering, 163, p.114299.

[7] Jr., S., April 08 2020. New TRISO Nuclear Mini-Reactors Will Be Safe: Program Manager. Retrieved September 13, 2020, from https://breakingdefense.com/2020/04/new-triso-nuclear-mini-reactors-will-be-safe-program-manager/

[8] Office of Nuclear Energy, 2019. TRISO Particles: The Most Robust Nuclear Fuel on Earth. July 9 2019. Retrieved from https://www.energy.gov/ne/articles/triso-particles-most-robust-nuclear-fuel-earth

[9] Bruna, Giovanni et. al., 2012. Overview of Generation IV (Gen IV) Reactor Designs - Safety and Radiological Protection Considerations.

[10] Corliss, William, 1971. Nuclear Reactors for Space Power. United States Atomic Energy Commission. Technical report.

[11] Demkowicz, Paul, TRISO Fuel: Design, Manufacturing, and Performance, NRC HTGR Training. INL, ART. July 16-17, 2019

[12] Rooyen, Isabella J Van Rooyen et. al. Microstructure and Fission Product Distribution Examination in the UCO Kernel of TRISO Fuel Particles. INL-DOE. Oct. 2018.

[13] Besmann, T. M., Shin, D., Lindemer, T. B., 2012. Uranium nitride as LWR TRISO fuel: Thermodynamic modeling of U–C–N. Journal of Nuclear Materials, 427(1-3), 162-168. doi:10.1016/j.jnucmat. 2012.04.021.

[14] Nosek, A., Conzen, J., Doescher, H., Martin, C., &; Blanchard, J., 2007. Thermomechanics of candidate coatings for advanced gas reactor fuels. Journal of Nuclear Materials, 371(1-3), 288-303. doi:10.1016/j.jnucmat.2007.05.014

[15] D.A. Brown, et. al., 2018. "ENDF/B-VIII.0: The 8th Major Release of the Nuclear Reaction Data Library with CIELO-project Cross Sections, New Standards and Thermal Scattering Data", Nuclear Data Sheets, 148: pp. 1-142.

[16] Mason, Lee, 2001/02/01. A Comparison of Brayton and Stirling Space Nuclear Power Systems for Power Levels from 1 Kilowatt to 10 Megawatts, DO - 10.1063/1.1358045

[17] Todreas, N. E., Kazimi, M. S. (1990). Nuclear systems. thermal hydraulic fundamentals. Bristol, PA: Hemisphere.

[18] Z. Li, J. Sun, M. Liu, M. Lang, and L. Shi, “Design of a hundred-kilowatt level integrated gas-cooled space nuclear reactor for deep space application,” Nuclear Engineering and Design, vol. 361, p. 110569, 2020.

[19] Mason, Lee S., Schreiber, Jeffery G., 2007. “A Historical Review of Brayton and Stirling Power Conversion Technologies for Space Applications” NASA Glenn Research Center.

[20] Nuclear Fuel Cycle and Materials Section, High Temperature Gas Cooled Reactor Fuels and Materials (2010). Vienna; IAEA. ISBN 978-92-0-153110-2, ISSN 1684-2073

[21] NASA. (n.d.). WTP: Shuttle: Cargo Bay. NASA. https://pds.nasa.gov/planets/captions/shuttle/sts03.htm: :text=The%20bay%2C%2018.3%20m%20long,and%20shapes%20in%20one%20mission.

[22] Zellner, N. E. (2016). Lunar Regolith: Materials. Encyclopedia of Lunar Science, 1–7. https://doi.org/10.1007/978-3-319-05546-6_82-1

[23] Eppstein, D. (n.d.). The Geometry Junkyard. Retrieved February 27, 2021, from https://www.ics.uci.edu/ eppstein/junkyard/

[24] Specht, E. (2013, October 18). The Best Known Packings of Equal Circles in a Square. Uni-Magdeburg. http://hydra.nat.uni-magdeburg.de/packing/csq/csq.html.

[25] U.S. Department of Energy. (2021, January 5). X-energy is Developing a Pebble Bed Reactor That They Say Can’t Melt Down. Energy.gov. https://www.energy.gov/ne/articles/x-energy-developing-pebble-bed-reactor-they-say-cant-melt-down.

[26] Los Alamos National Laboratory, Hu, J., Uddin, R., LA-UR-10-004423D Thermal Modeling of TRlSO Fuel Coupled with Neutronic Simulation (n.d.). Intended for International Congress on Advance in Nuclear Power Plants meeting

[27] Silva, C. M., Hunt, R. D., Snead, L. L., Terrani, K. A. (2014). Synthesis of Phase-Pure U2N3 Microspheres and Its Decomposition into UN. Inorganic Chemistry, 54(1), 293–298. https://doi.org/10.1021/ic502457n

[28] McMurray, J. W., Lindemer, T. B., Brown, N. R., Reif, T. J., Morris, R. N., Hunn, J. D. (2017). Determining the minimum required uranium carbide

content for HTGR UCO fuel kernels. Annals of Nuclear Energy, 104, 237–242. https://doi.org/10.1016/j.anucene.2017.02.023

[29] Schilthelm, S., McIntyre, B., Sloan, S. (2019). (tech.). Uranium Oxycarbide (UCO) Tristructural Isotropic (TRISO) Coated Particle Fuel Performance . Lynchburg, VA: BWXT Nuclear Energy, Inc. .

[30] Terrani, K. A., Jolly, B. C., Harp, J. M. (2020). Uranium nitride tristructural-isotropic fuel particle. Journal of Nuclear Materials, 531, 152034. https://doi.org/10.1016/j.jnucmat.2020.152034

[31] De Coninck, R., Van Lierde, W., Gijs, A. (1975). Uranium carbide: Thermal diffusivity, thermal conductivity and spectral emissivity at high temperatures. Journal of Nuclear Materials, 57(1), 69–76. https://doi.org/10.1016/0022-3115(75)90179-8

[32] S.B. Ross, M.S. El-Genk. Thermal conductivity correlation for uranium nitride fuel between 10 and 1923 K, J. Nucl. Mater. 151 (1988) 313e317.

[33] Thermal and Nuclear Power Plants/Handbook ed. by A.V. Klimenko and V.M. Zorin. MEI Press, 2003

[34] Westrum, E. F., Barber, C. M. (1966). Uranium Mononitride: Heat Capacity and Thermodynamic Properties from 5° to 350°K. The Journal of Chemical Physics, 45(2), 635–639. https://doi.org/10.1063/1.1727621

[35] Ekberg, C., Ribeiro Costa, D., Hedberg, M., Jolkkonen, M. (2018). Nitride fuel for Gen IV nuclear power systems. Journal of Radioanalytical and Nuclear Chemistry, 318(3), 1713–1725. https://doi.org/10.1007/s10967-018-6316-0

[36] Oetting, F. L., Navratil, J. D., Storms, E. K. (1973). The chemical thermodynamic properties of nuclear materials: (II) High temperature enthalpy of the uranium carbides. Journal of Nuclear Materials, 45(4), 271–283. https://doi.org/10.1016/0022-3115(73)90161-X

[37] Dai, Z., Wang, C., Zhang, D., Tian, W., Qiu, S., Su, G. H. (2021). Design and analysis of a free-piston stirling engine for space nuclear power reactor. Nuclear Engineering and Technology, 53(2), 637–646. https://doi.org/10.1016/j.net.2020.07.011

[38] McCarty, R. D. (1972). Thermophysical properties of helium-4 from 2 to 1500 K with pressures to 1000 atmospheres. U.S. G.P.O.

APPENDIX

Figure A.1: Run data from Figure 2.4 (A)

Multiplyer	**Kernel**	**Buffer**	**iPyC**	**SiC**	**oPyC**	**Keff**	**Error**	**Reactivity**
0.6	0.015	0.021	0.0231	0.0252	0.0276	0.57003	0.00046	-0.75429
0.7	0.0175	0.0245	0.02695	0.0294	0.0322	0.70866	0.00039	-0.41111
0.8	0.02	0.028	0.0308	0.0336	0.0368	0.81732	0.00042	-0.22351
0.9	0.0225	0.0315	0.03465	0.0378	0.0414	0.89753	0.00041	-0.11417
1	0.025	0.035	0.0385	0.042	0.046	0.95506	0.00062	-0.04705
1.1	0.0275	0.0385	0.04235	0.0462	0.0506	0.98935	0.00062	-0.01076
1.2	0.03	0.042	0.0462	0.0504	0.0552	1.0106	0.00062	0.010489
1.3	0.0325	0.0455	0.05005	0.0546	0.0598	1.02172	0.00066	0.021258
1.4	0.035	0.049	0.0539	0.0588	0.0644	1.02419	0.00062	0.023619
1.5	0.0375	0.0525	0.05775	0.063	0.069	1.02015	0.0006	0.019752

Figure A.2: Run data from Figure 2.4 (B)

Multiplyer	Kernel	Buffer	iPyC	SiC	oPyC	Keff	Error	Reactivity
0.6	0.021086	0.02952	0.032472	0.035424	0.038798	0.85667	0.00042	-0.16731
0.7	0.022198	0.031077	0.034184	0.037292	0.040844	0.8893	0.00043	-0.12448
0.8	0.023208	0.032491	0.03574	0.038989	0.042703	0.91687	0.00042	-0.09067
0.9	0.024137	0.033792	0.037171	0.040551	0.044413	0.93643	0.00044	-0.06789
1	0.025	0.035	0.0385	0.042	0.046	0.95449	0.00044	-0.04768
1.1	0.025807	0.03613	0.039743	0.043356	0.047485	0.96701	0.00043	-0.03412
1.2	0.026566	0.037193	0.040912	0.044632	0.048882	0.97886	0.00044	-0.0216
1.3	0.027285	0.038199	0.042019	0.045839	0.050204	0.98737	0.00045	-0.01279
1.4	0.027967	0.039154	0.04307	0.046985	0.05146	0.99529	0.00044	-0.00473
1.5	0.028618	0.040065	0.044071	0.048078	0.052657	1.00024	0.00042	0.00024

Figure A.3: Run data from Figure 2.4 (C)

Multiplyer	Kernel	Buffer	iPyC	SiC	oPyC	Keff	Error	Reactivity
0.2	0.033	0.035	0.0385	0.042	0.046	1.02913	0.00045	0.028305
0.3	0.032	0.035	0.0385	0.042	0.046	1.02913	0.00045	0.028305
0.4	0.031	0.035	0.0385	0.042	0.046	1.02259	0.00042	0.022091
0.5	0.03	0.035	0.0385	0.042	0.046	1.01569	0.00044	0.015448
0.6	0.029	0.035	0.0385	0.042	0.046	1.00813	0.00046	0.008064
0.7	0.028	0.035	0.0385	0.042	0.046	0.9977	0.00045	-0.00231
0.8	0.027	0.035	0.0385	0.042	0.046	0.98562	0.00043	-0.01459
0.9	0.026	0.035	0.0385	0.042	0.046	0.97211	0.00046	-0.02869
1	0.025	0.035	0.0385	0.042	0.046	0.95449	0.00044	-0.04768
1.1	0.024	0.035	0.0385	0.042	0.046	0.93347	0.00044	-0.07127
1.2	0.023	0.035	0.0385	0.042	0.046	0.90988	0.00042	-0.09905

Figure A.4: Run data from Figure 2.4 (D)

Multiplier	Porosity	Density	Keff	Error	Reactivity
0.6	0.3	0.57	0.95303	0.00043	-0.04928
0.7	0.35	0.665	0.9532	0.00042	-0.0491
0.8	0.4	0.76	0.95268	0.00046	-0.04967
0.9	0.45	0.855	0.95351	0.00044	-0.04876
1	0.5	0.95	0.95281	0.00043	-0.04953
1.1	0.55	1.045	0.95285	0.0004	-0.04948
1.2	0.6	1.14	0.95262	0.00042	-0.04974
1.3	0.65	1.235	0.95512	0.00045	-0.04699
1.4	0.7	1.33	0.95403	0.00045	-0.04819
1.5	0.75	1.425	0.95413	0.00044	-0.04808

Figure A.5: Run data from Figure 2.4 (E)

Percentage O	**ZAID**	**Keff**	**Error**	**Reactivity**
0	92235 0.2 92238 0.8 6012 2.0	0.95842	0.00041	-0.04338
10	92235 0.2 92238 0.8 6012 1.8 8016 0.2	0.9579	0.00044	-0.04395
20	92235 0.2 92238 0.8 6012 1.6 8016 0.4	0.95673	0.00043	-0.04523
30	92235 0.2 92238 0.8 6012 1.4 8016 0.6	0.95703	0.00047	-0.0449
40	92235 0.2 92238 0.8 6012 1.2 8016 0.8	0.95512	0.00045	-0.04699
50	92235 0.2 92238 0.8 6012 1.0 8016 1.0	0.95526	0.00044	-0.04684
60	92235 0.2 92238 0.8 6012 0.8 8016 1.2	0.95468	0.00043	-0.04747
70	92235 0.2 92238 0.8 6012 0.6 8016 1.4	0.95369	0.00043	-0.04856
80	92235 0.2 92238 0.8 6012 0.4 8016 1.6	0.95423	0.00045	-0.04797
90	92235 0.2 92238 0.8 6012 0.2 8016 1.8	0.95284	0.00042	-0.04949
100	92235 0.2 92238 0.8 8016 2.0	0.95295	0.00045	-0.04937

Table A.6: Reactor design iteration dimension effects on multiplication factor

TRISO Reactor Name	Shape	Length (cm)	Radius (cm)	Stacking Method	Reactor Thickness (cm)	Reactor Radius (cm)	Absorber Thickness (cm)	K	std
C.01.01	Cylinder	150	21	Method 1	none	none	none	0.22059	0.00026
C.01.02	Cylinder	300	42	Method 1	none	none	none	0.89168	0.00044
C.01.03	Cylinder	300	84	Method 1	none	none	none	1.4252	0.00041
C.01.04	Cylinder	300	60	Method 1	none	none	none	1.21026	0.00044
C.01.05	Cylinder	228	63	Method 1	none	none	none	1.22532	0.00048
C.01.06	Cylinder	198	57	Method 1	none	none	none	1.14718	0.00046
C.02.01	Cylinder	198	57	Method 2	none	none	none	1.12921	0.00045
C.02.01	Diamond-Cylinder	198	57	Method 2	none	none	none	1.11572	0.00043
C.03.01	Diamond-Cylinder	198	57	Method 1	none	none	none	1.13292	0.00043
C.03.06.ON	Diamond-Cylinder	89.56	62	Method 1	14.88	76.88	1.378	0.76787	0.00042
C.04.01.ON	Diamond-Cylinder	101.11	70	Method 1	16.8	86.8	1.556	0.9002	0.00044
C.04.02.OFF	Diamond-Cylinder	101.11	70	Method 1	16.8	86.8	3.298	0.89932	0.00044
C.04.03.ON	Diamond-Cylinder	115.56	80	Method 1	19.2	99.2	3.769	1.02367	0.00046
C.05.01	Diamond-Cylinder	101.11	70	Method 1	19.95	89.95	3.916	0.90031	0.00043
C.05.02	Diamond-Cylinder	101.11	70	Method 1	19.95	89.95	1.847	0.901	0.00046
C.05.03	Diamond-Cylinder	101.11	70	Method 1	19.95	89.95	0.924	0.90015	0.00045
C.05.04	Diamond-Cylinder	175	70	Method 1	19.95	89.95	2.882	0.89941	0.00043
C.05.05	Diamond-Cylinder	175	70	Method 1	19.95	89.95	1.385	0.89975	0.00044
C.05.06	Diamond-Cylinder	211	75	Method 1	21.375	96.375	1.979	1.0196	0.00044
C.06.01(Water w B)	Diamond-Cylinder	211	75	Method 1	21.375	96.375	1.979	0.6213	0.01187
C.06.01(Water w/o B)	Diamond-Cylinder	211	75	Method 1	21.375	96.375	1.979	0.63241	0.01107